

**Size effects on elasticity, yielding, and fracture of silver nanowires: *In situ* experiments**Yong Zhu,<sup>1,\*</sup> Qingquan Qin,<sup>1</sup> Feng Xu,<sup>1</sup> Fengru Fan,<sup>2</sup> Yong Ding,<sup>2</sup> Tim Zhang,<sup>3</sup> Benjamin J. Wiley,<sup>3</sup> and Zhong Lin Wang<sup>2</sup><sup>1</sup>*Department of Mechanical and Aerospace Engineering, North Carolina State University, Raleigh, North Carolina 27695, USA*<sup>2</sup>*School of Materials Science and Engineering, Georgia Institute of Technology, Atlanta, Georgia 30332, USA*<sup>3</sup>*Department of Chemistry, Duke University, Durham, North Carolina 27708, USA*

(Received 31 August 2011; published 30 January 2012)

This paper reports the quantitative measurement of a full spectrum of mechanical properties of fivefold twinned silver (Ag) nanowires (NWs), including Young's modulus, yield strength, and ultimate tensile strength. *In-situ* tensile testing of Ag NWs with diameters between 34 and 130 nm was carried out inside a scanning electron microscope (SEM). Young's modulus, yield strength, and ultimate tensile strength all increased as the NW diameter decreased. The maximum yield strength in our tests was found to be 2.64 GPa, which is about 50 times the bulk value and close to the theoretical value of Ag in the  $\langle 110 \rangle$  orientation. The size effect in the yield strength is mainly due to the stiffening size effect in the Young's modulus. Yield strain scales reasonably well with the NW surface area, which reveals that yielding of Ag NWs is due to dislocation nucleation from surface sources. Pronounced strain hardening was observed for most NWs in our study. The strain hardening, which has not previously been reported for NWs, is mainly attributed to the presence of internal twin boundaries.

DOI: 10.1103/PhysRevB.85.045443

PACS number(s): 62.25.-g

**I. INTRODUCTION**

Bulk silver (Ag) exhibits the highest electrical and thermal conductivity among metals. As such, Ag nanowires (NWs) are expected to be outstanding conductors in nanoscale electronic devices.<sup>1,2</sup> Of particular note is that flexible/stretchable electronics based on nanomaterials have received much recent attention.<sup>3,4</sup> Ag NWs hold promising potential as flexible electrodes.<sup>5</sup> In addition, Ag NWs exhibit an interesting optical property known as surface plasmon resonance, which occurs as a result of the coherent oscillation of the conduction electrons upon interaction with electromagnetic fields.<sup>6</sup> The plasmonic properties of Ag NWs have been used in a wealth of applications, including biosensing<sup>7</sup> and plasmonic waveguiding.<sup>8</sup> Axial strain or bending deformation has been found to significantly affect the surface plasmon resonance of Ag NWs.<sup>8,9</sup> From an engineering perspective, mechanical properties of Ag NWs play an important role in the functionality and reliability of the above device applications.

Previous experimental studies on mechanical properties of Ag NWs have focused on elasticity using testing methods such as three-point bending<sup>10,11</sup> and nanoindentation.<sup>12,13</sup> In spite of large data scatter, a stiffening trend (i.e. increase in Young's modulus with decrease in NW diameter) was generally observed. However, experimental measurements on the plasticity and failure of Ag NWs are rare and indirect.<sup>10,13</sup> Tensile testing is a direct experimental method to obtain a full spectrum of mechanical properties (including elasticity, plasticity and failure). Indeed, such a full spectrum of mechanical properties under tensile loading has been investigated by atomistic simulations.<sup>14</sup> The Ag NWs to be studied in this paper possess a well-defined fivefold twinned microstructure. Ag NWs thus provide a model system for studying the combined effects of sample dimensions and internal interfaces on the mechanical properties of nanomaterials.

In this paper, we report quantitative stress-strain measurements of individual fivefold twinned Ag NWs (30 to 130 nm in diameter) using *in-situ* tensile tests inside a scanning electron microscope (SEM). In addition to the stiffening size effect in

the Young's modulus, we found that the yield strength and ultimate tensile strength (UTS) both increased as the NW diameter decreased. The maximum yield strength and UTS in our tests were 2.64 GPa (close to the theoretical strength of Ag in the  $\langle 110 \rangle$  orientation) and 4.84 GPa, respectively. The size effect in the yield strength is attributed to the increase in the Young's modulus. Yield strain scales reasonably well with the NW surface area, which reveals that yielding of Ag NWs is due to dislocation nucleation from surface sources. Pronounced strain hardening was observed for most NWs in our study. The strain hardening, which has not previously been observed for NWs, is mainly attributed to the presence of internal twin boundaries.

**II. EXPERIMENTAL PROCEDURE**

Fivefold twinned Ag NWs were synthesized by reducing AgNO<sub>3</sub> with ethylene glycol (EG) in the presence of polyvinyl pyrrolidone (PVP). Fivefold twinned Ag NWs were obtained by carefully controlling the synthesis conditions, including the temperature, the concentrations of AgNO<sub>3</sub> and PVP, as well as the presence of trace contaminants, such as iron and chloride ions. Detailed description of the NW synthesis process can be found elsewhere.<sup>1</sup> The solution of Ag NWs was diluted with deionized water (five times by volume) and then purified by centrifugation at 3000 rpm for about 20 minutes to remove PVP and other unwanted materials, such as Ag nanoparticles. This washing step was repeated multiple times to obtain the desired results. Purified Ag NWs were dropped on a transmission electron microscopy (TEM) grid and a clean silicon wafer for TEM observation and *in-situ* SEM testing, respectively.

The TEM observation was carried out in JEOL 4000EX. Figure 1(a) shows a low-magnification TEM image of Ag NWs with diameters  $\sim 80$  nm. The Ag NWs are straight and uniform in width. Typically, Ag NWs synthesized by this method have a multiply twinned, pentagonal structure with smooth, faceted surfaces.<sup>1,2</sup> The microstructure of fivefold twinned NWs is

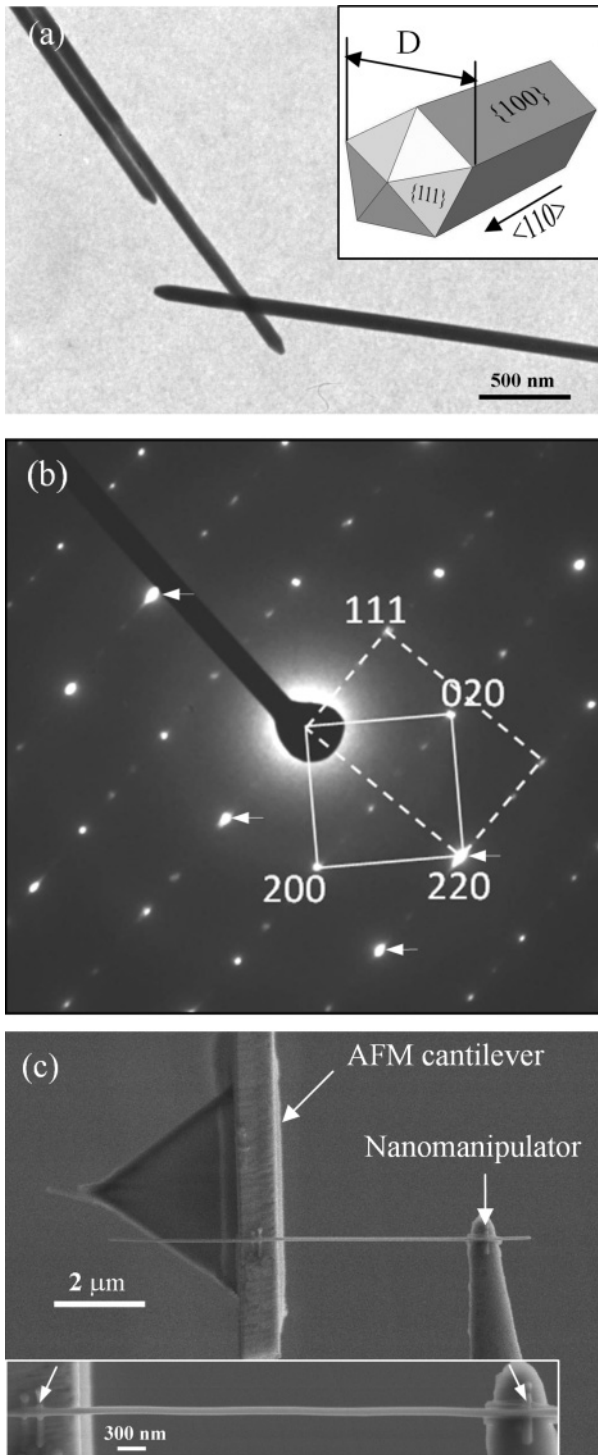


FIG. 1. (a) Low-magnification TEM image of Ag NWs with a diameter  $\sim 80$  nm. Inset of (a) shows a 3D schematic of fivefold twinned NW and the effective diameter  $D$  used in this study. (b) SAED of an Ag NW. The indexed diffraction pattern corresponds to the overlapping of two zone axes,  $[001]$  (solid box) and  $[1\bar{1}2]$  (dashed box). The direction of the electron beam is perpendicular to one of the  $\{100\}$  side facets, as shown in panel (a). Elongated diffraction spots (arrows) are indicative of elastic strain in the NW. (c) SEM image showing the tensile test of a single Ag NW. Inset of (c) shows a high-resolution SEM image of the NW for strain measurement. Two arrows indicate the clamps by EBID of carbonaceous materials.

well documented.<sup>1,2,15,16</sup> The selected area electron diffraction (SAED) pattern [Fig. 1(b)] confirms that the NWs are grown in the  $\langle 110 \rangle$  direction and contain fivefold twins parallel to their longitudinal axis; the five twin boundaries are along  $\{111\}$  planes, and the five surface facets are along  $\{100\}$  planes. The NWs are elastically strained and might contain stacking faults and dislocations, especially at the core area of the NWs, since the five subunits cannot make  $360^\circ$  (i.e. the angle between two  $\{111\}$  planes is  $70.52^\circ$ , and five subunits can only make  $352.6^\circ$ ).<sup>15</sup> Some diffraction spots [arrow in Fig. 1(b)] are elongated, which is evidence of the elastic strain.<sup>16</sup>

The tensile tests were performed using a recently developed *in-situ* SEM nanomechanical testing setup.<sup>17–19</sup> The force was applied using a nanomanipulator (Klocke Nanotechnik, Germany) on one side of the freestanding specimen and was measured on the other side using an AFM cantilever. The specimen was clamped on the nanomanipulator tip and the AFM cantilever using electron-beam-induced deposition (EBID) of carbonaceous materials in the SEM<sup>17,20</sup> [Fig. 1(c)]. The drop-cast method used to prepare the NW samples ensures the NWs are perpendicular to the electron beam; thus, no out-of-plane rotation is coupled to the tension, and the strain measurement should be accurate. A small in-plane rotation might occur during the tension process as a result of the deflection of the AFM cantilever. We carefully selected AFM cantilevers with relatively large stiffness to ensure such in-plane rotation is negligible.<sup>17</sup> The specimen was then loaded in tension until failure to investigate the full spectrum of mechanical properties, including elastic, plastic, and failure properties. A series of SEM images were taken during the tension tests. Both force and elongation were measured from the images and converted to stress and strain, respectively. Force was obtained by multiplying the force sensor's (AFM cantilever's) displacement by its calibrated stiffness. The resolution of the force sensor used in this study was  $5.25 \pm 0.38$  nN. For NWs with diameters ranging from 34 to 130 nm, the stress resolution ranged from 5.78 to 0.37 MPa. Here the NW diameter is measured from the projected view in the SEM, which is the distance between two nonadjacent vertices [as shown in the inset of Fig. 1(a)] due to the pentagonal cross section. The real cross-sectional area,  $5D^2/(8 \sin 72^\circ)$  (where  $D$  is the NW diameter), is used to calculate the stress. The NW elongation was measured by digital image correlation of the SEM images; additional SEM images with high magnification were taken at each loading step to increase the strain resolution [as shown in the inset of Fig. 1(c)]. As an NW typically spans 1500–1800 pixels in length and we can measure the NW elongation with the resolution of half a pixel, the strain resolution is about 0.03%. After each test, we carefully examined both clamps to ensure there was no slippage between the NW and the clamps, following a procedure we developed previously.<sup>17</sup>

### III. RESULTS AND DISCUSSION

Figure 2(a) shows a typical stress-strain behavior of Ag NWs. The first, second, and third unloading occurred at a strain of 0.7%, 1.5%, and 3.0%, respectively. It can be seen that the first loading and unloading curves followed nearly identical paths. No residual plastic deformation was

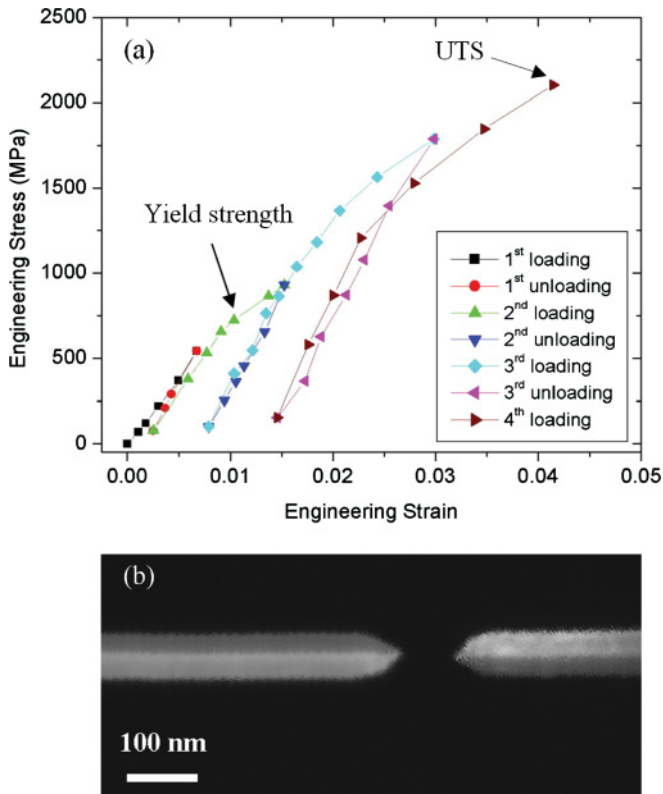


FIG. 2. (Color online) (a) Stress-strain of an Ag NW with diameter of 69 nm under tensile loading, where the Young’s modulus, yield strength, and ultimate tensile strength (UTS) are 90, 0.72, and 2.10 GPa, respectively, and yield strain and strain at UTS are 0.92 and 4.14, respectively. (b) SEM image showing the fracture surfaces of the Ag NW.

observed when the NW was fully unloaded. By contrast, upon unloading at strains larger than 1.5%, the NW underwent plastic deformation with pronounced strain hardening, but the high-magnification SEM images during the testing showed no sign of diameter reduction or necking prior to NW failure. After failure, a close examination of the NW fracture ends [Fig. 2(b)] showed that there is no apparent diameter reduction (i.e. no large-scale yielding) along the NW except very close

to the fracture surface. This observation is consistent with the stress-strain data where the plasticity is limited compared to bulk face-centered cubic (FCC) metals. Both fractography and stress-strain data suggested that the dislocation-induced shear is localized, which agrees with molecular dynamics (MD) simulations of fivefold twinned Ag NWs.<sup>14</sup> Tension tests of all the NWs at different diameters were conducted following the same procedure with multiple loading/unloading cycles. A nearly constant strain rate ( $\sim 0.1\%/s$ ) was maintained for all the tests. Note that our experiments were under load control, so the strain softening regime succeeding the UTS was not captured. Engineering stress and strain are plotted in this paper.

To study the size effects on the mechanical properties of Ag NWs, a total of 13 NWs with diameters ranging from 34 to 130 nm were tested. The NW dimensions and measured properties are listed in Table I. Figure 3(a) shows both the yield strength and the UTS as functions of the NW diameter. Since no apparent yielding was observed in our tests, the yield strength was defined using the 0.2% offset method. The UTS was defined as the maximum stress that a NW can withstand in tensile test. In a typical stress-strain curve, as shown in Fig. 2(a), the maximum stress value prior to the NW breakage was taken as the UTS for this NW. The yield strength was strongly size dependent, increasing from 0.71 to 2.64 GPa as the diameter decreased from 130 down to 34 nm. The highest yield strength of Ag NWs was about 50 times higher than the bulk value (54 MPa) and was close to the theoretical tensile strength of Ag in the  $\langle 110 \rangle$  direction, which was calculated to be 3.5 GPa following the Schmid factor analysis of the  $\{111\}/\langle 112 \rangle$  slip system.<sup>21</sup> The UTS was higher than the yield strength for most of the tested NWs, which indicates the Ag NWs underwent strain hardening. Only two out of the 13 NWs showed the same UTS as the yield strength. This is likely due to a small increase in stress between the two events, which was not captured in our experiments.

Figure 3(b) shows a log-log plot of the yield strength as a function of the NW diameter. This plot indicates that the Ag NWs in the diameter range as tested obey the widely observed power-law size effect, with a power-law exponent of 0.66, well within the previously reported range.<sup>22</sup> Plasticity of micro/nanopillars has been extensively studied in recent years.<sup>22,23</sup> In general, strength increases as the pillar diameter

TABLE I. Dimensions and mechanical properties of 13 Ag NWs under tension.

Sample number	Diameter (nm)	Length ( $\mu\text{m}$ )	Young’s modulus (GPa)	Yield strain (%)	Yield strength (GPa)	UTS (GPa)
1	34	2.09	176	1.25	1.71	3.13
2	38	1.94	171	1.44	2.64	4.84
3	42	4.33	148	1.64	2.35	2.35
4	42	3.87	138	0.98	1.38	1.98
5	55	4.64	120	1.25	1.39	1.86
6	69	3.83	90	0.92	0.72	2.10
7	72	5.44	104	1.02	1.14	1.29
8	72	5.72	103	1.03	1.11	1.35
9	80	4.67	94	1.55	1.41	1.41
10	96	2.11	86	1.47	1.26	1.36
11	96	2.81	94	1.35	1.24	1.53
12	110	2.69	73	1.63	1.00	1.18
13	130	5.73	81	1.00	0.71	0.87

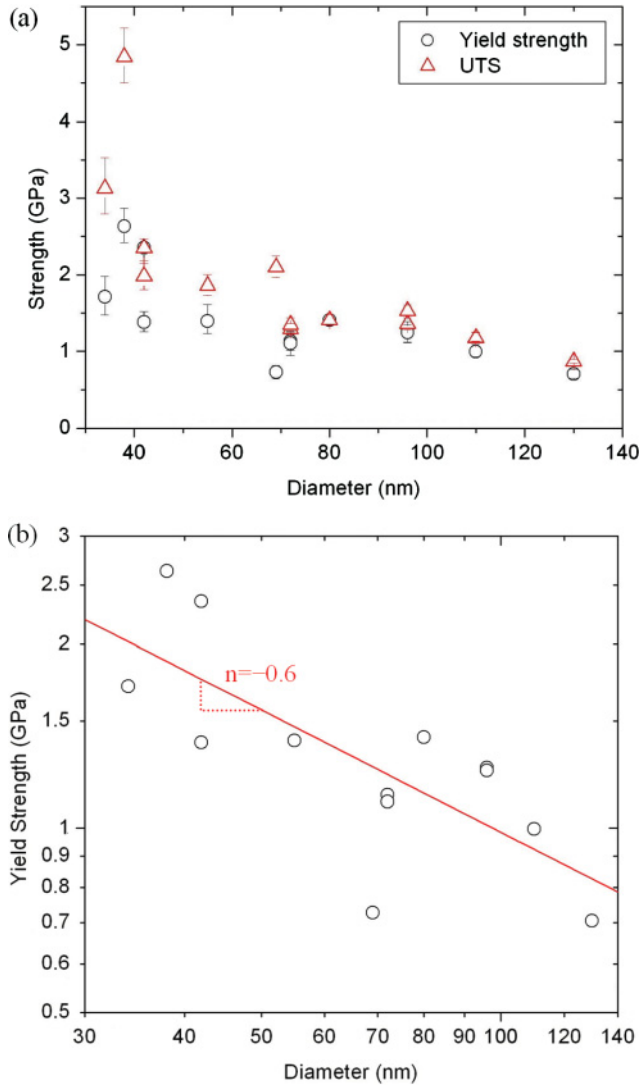


FIG. 3. (Color online) (a) Yield strength and ultimate tensile strength (UTS). (b) Log-log plot of true yield strength as a function of NW diameter. The data show a power-law trend (shown by red/dark gray line) with  $n = -0.66$ .

decreases. For micropillars, plasticity occurs through the activation of single-arm sources (or truncated Frank-Read sources). A power-law size effect was generally observed with the power-law exponent between 0.5 and 1. For small nanopillars (e.g. diameter less than  $\sim 200$  nm), plasticity occurs through dislocation nucleation from surface sources. A weaker size effect was predicted<sup>24</sup> and recently observed experimentally.<sup>25</sup> Thus, the power-law size effect in yield strength (e.g. via the single-arm source mediated mechanisms) is somewhat contradictory to the fact that the NW diameters are well below 200 nm.

To further probe the mechanism for the size effect in the yield strength of Ag NWs, the yield strain is plotted as a function of the NW diameter, see Fig. 4(a). Yield strains show large scatter ranging from 0.92% to 1.64%, with almost no correlation with the diameter. The yield strain is plotted as a function of the NW side surface area, see Fig. 4(b). This

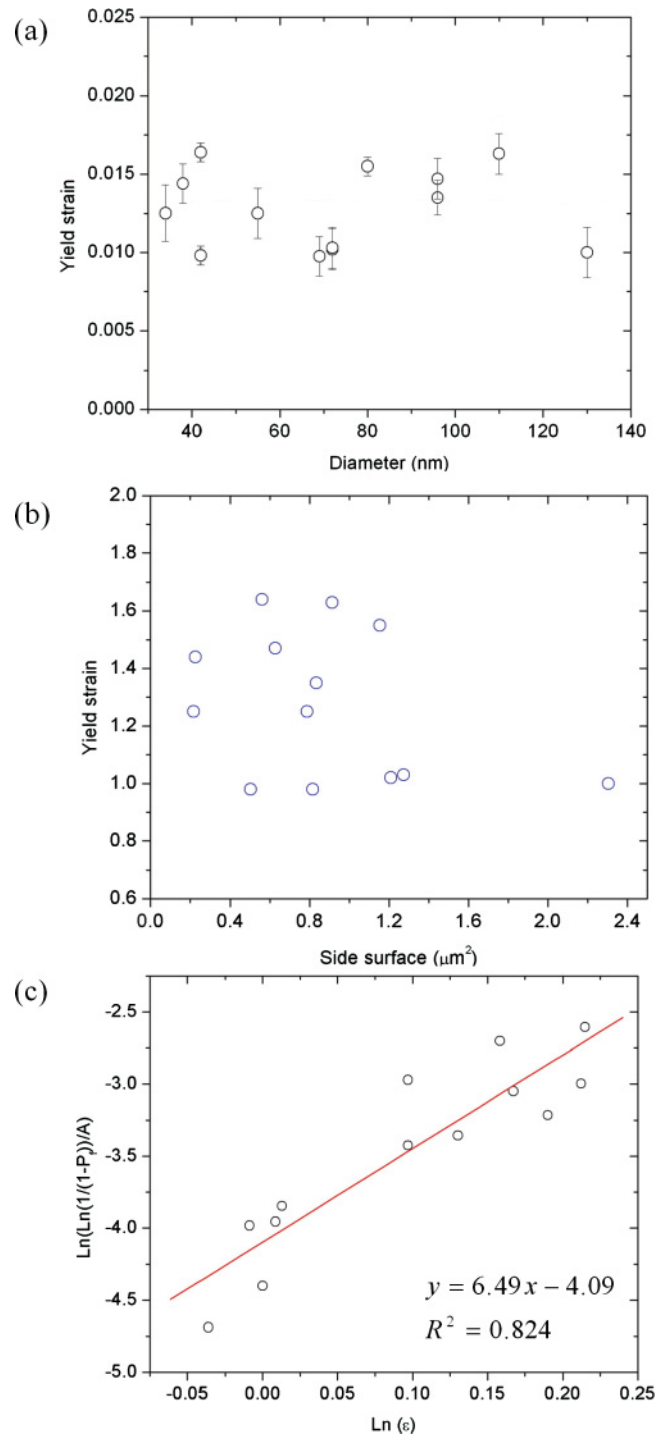


FIG. 4. (Color online) Yield strain as a function of (a) NW diameter and (b) NW side surface. (c) Plot of the Weibull statistics. Probabilities ( $P_f$ ) are calculated as  $P_f(\epsilon_i) = \frac{i-1/2}{N}$ , where  $N$  is the total number of specimens tested, and the measured yield strains are ranked in ascending order.

plot shows a general trend that yield strain increases with decreasing surface area but suggests that this size effect is quite weak, which is nevertheless in line with the mechanism of dislocation nucleation from free surfaces (surface sources<sup>24</sup>). Note that the aspect ratio of NWs was not constant in this study. A Weibull-type weakest-link probabilistic model was applied

to verify if the observed variation can be associated with the surface sources.<sup>26</sup> Weibull statistics assumes the probability of failure  $P_f$  for a specimen of surface area  $A$  under uniaxial tension as

$$P_f = 1 - \exp \left[ - \left( \frac{\varepsilon_f}{\varepsilon_{0A}} \right)^m A \right] \quad (1)$$

where  $\varepsilon_f$  is the yield strain,  $\varepsilon_{0A}$  is the characteristic strain relative to unit surface area, and  $m$  is the Weibull modulus. The Weibull statistics applied to this set of yield strain data with respect to the surface area is shown in Fig. 4(c).

The coefficient of correlation for NW side surface area is  $\sim 82\%$ , in contrast to that for the NW volume ( $\sim 64\%$ ). This indicates that yield strain, to some extent, is associated with the side surface area of the NWs. Better correlation could be achieved if the number of experiments was increased. Size effect on yield strain of NWs is likely caused by the statistical nature of surface dislocation sources, assuming the first dislocation is nucleated from the weakest-link source.<sup>27</sup> Our results corroborate atomistic simulations of fivefold twinned NWs, where yielding occurs as partial dislocations nucleate from surfaces.<sup>14,28</sup> While the weakest-link type of models is conventionally applied to brittle fracture, they could play an important role in the yielding at small scales, indeed as applied to metal whiskers by Brenner<sup>29</sup> and recently to nanopillars<sup>30</sup> and NWs.<sup>31</sup> The increased sensitivity to temperature and strain rate (related to the dislocation nucleation from surfaces) might account for the large data scatter in our yield strain as observed here.

The Young's modulus is also plotted as a function of the NW diameter, as shown in Fig. 5. The first unloading slope in a stress-strain curve was used to calculate the Young's modulus in our study. A linear fitting was applied to the first unloading curve. Errors of the Young's modulus measurement could come from the strain and stress measurements as well as the fitting (see error bars in Fig. 5). The Young's modulus of bulk Ag in the  $\langle 110 \rangle$  direction (84 GPa) is plotted as a dashed line for comparison.<sup>32</sup> A stiffening trend was observed for

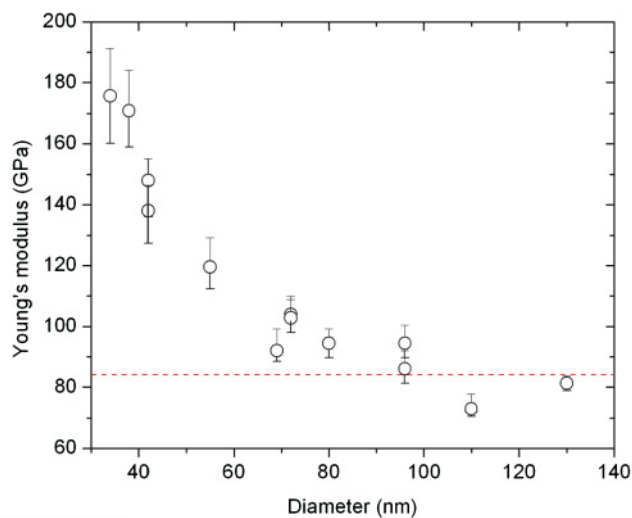


FIG. 5. (Color online) Young's modulus as a function of NW diameter. The dash line represents the Young's modulus of bulk Ag in  $\langle 110 \rangle$  direction.

NWs with diameters less than 80 nm; the Young's modulus continuously increased with the decreasing diameter down to 34 nm. For Ag NWs with diameters over  $\sim 80$  nm, their Young's moduli appeared to be slightly lower than the bulk value. The Young's modulus results from our *in-situ* SEM tensile tests agree well with those from the AFM tests.<sup>11,33</sup> Note that our strain was directly measured from the SEM images, so the machine compliance did not contribute to our measurement of Young's modulus.

The observed size effect on elasticity of Ag NWs is generally a result of their large surface area to volume ratio,<sup>34</sup> mainly surface elasticity<sup>18,35</sup> and/or bulk nonlinear elasticity (due to surface stress).<sup>36,37</sup> Though our results are in good agreement with other experimental results,<sup>11,33</sup> we do note that there is a substantial gap between the experiments and the atomistic simulations in terms of the critical diameter where the elasticity size effect becomes marked.<sup>14</sup> One significant reason is the difference in aspect ratio (length/diameter). The NW aspect ratio in atomistic simulations is much smaller than those in our experiments. As aforementioned, the aspect ratio was not intended to be kept as constant in this study. Park *et al.* predicted that the aspect ratio plays an important role in the elasticity size effect in NWs; the small aspect ratio used in atomistic simulations could underestimate the size effect.<sup>38</sup> Furthermore, the fivefold twin structure could play a critical role in the elasticity size effect. Recent atomistic simulations found that the intrinsic strain state leads to a much stronger size effect in elasticity for fivefold twinned NWs than twin-free NWs.<sup>39</sup> It is of additional note that the embedded atom method (EAM) potential commonly used in MD simulations might underestimate the Young's modulus to a certain degree.<sup>39,40</sup>

Yield (or fracture) strength is simply equal to Young's modulus multiplied by yield (or fracture) strain. Brittle NWs, such as Si and ZnO, have been found to exhibit strong size effect in Young's modulus.<sup>17,18,41,42</sup> It seems more fundamental to correlate fracture strain with (surface) defects instead of the commonly used fracture strength, so as to eliminate the contribution of Young's modulus.<sup>43</sup> This argument is likely also applicable to ductile NWs, such as the Ag NWs, where yield strain can be correlated with side surface area.

In addition to the high yield strength and UTS, an intriguing mechanical behavior—strain hardening of NWs under tension—was observed. For micro/nanopillars (with diameters ranging from submicrometer to tens of micrometers) under compression, strain hardening was observed and was mainly attributed to limited dislocation sources and not much to the interaction of slip systems as in the macroscopic scale,<sup>44–46</sup> but recent experiments and simulations suggested that in single-crystalline nanopillars or NWs (with diameters typically less than  $\sim 200$  nm), dislocations are relatively easily annihilated at free surfaces before they have the opportunity to interact (e.g. the gliding dislocations travel only very short distances before annihilating at a free surface), leading to no strain hardening.<sup>24,47–49</sup> Nevertheless, our results clearly show the strain hardening in fivefold twinned Ag NWs [Fig. 2(a)]. Molecular dynamics simulations of fivefold twinned NWs predicted that partial dislocations are nucleated from surfaces and glide towards the NW center following a  $\{111\}/\langle 112 \rangle$  slip system.<sup>14,28</sup> The observed strain hardening in our case is likely due to the interaction between partial dislocations

and twin boundaries<sup>50</sup> in addition to the limited dislocation sources. Twin boundaries have been ascribed to the strain hardening observed in nanostructured materials<sup>51,52</sup> and NWs with orthogonally oriented twins.<sup>53</sup> A complete analysis of the observed strain hardening in Ag NWs requires a combined experimental and modeling investigation, which is currently underway.

#### IV. CONCLUSIONS

The elasticity, plasticity and failure of five-fold twinned Ag NWs with diameters between 34 and 130 nm were measured by *in situ* SEM tensile testing. In addition to the stiffening size effect in Young's modulus, we found that yield strength and ultimate tensile strength both increased as the NW diameter decreased. The size effect in yield strength was mainly attributed to the stiffening size effect in Young's modulus, which is in turn a result of the surface effect and the unique five-fold twin microstructure. Note that in our measurement of Young's modulus, the effect of machine compliance is excluded. Yield strain scales reasonably well with the NW surface area,

notwithstanding the scaling is quite weak when compared to the power-law relationship. Such a scaling confirms the yielding mechanism of dislocation nucleation from surface sources. Pronounced strain hardening was observed for most NWs in our study, which is hypothesized to result from the internal twin boundaries in addition to the limited dislocation sources. The present work provides valuable insight into the importance of both size and microstructure on the mechanical properties of NWs.

#### ACKNOWLEDGMENTS

This work was supported by NSF under Award No. CMMI-1030637. The *in-situ* SEM experiments were performed in the Analytical Instrumentation Facility at North Carolina State University. A portion of this research was conducted at the Center for Nanophase Materials Sciences, which is sponsored at Oak Ridge National Laboratory by the Office of Basic Energy Sciences, US Department of Energy. YZ thanks Prof. T. Zhu, Prof. H. C. Huang and Prof. H. S. Park for helpful discussions.

\*Corresponding author: Department of Mechanical & Aerospace Engineering, NCSU, 911 Oval Dr., Raleigh, NC 27695; yong\_zhu@ncsu.edu

<sup>1</sup>B. Wiley, Y. Sun, and Y. Xia, *Accounts Chem. Res.* **40**, 1067 (2007).

<sup>2</sup>K. K. Caswell, C. M. Bender, and C. J. Murphy, *Nano Lett.* **3**, 667 (2003).

<sup>3</sup>Z. Fan, J. C. Ho, T. Takahashi, R. Yerushalmi, K. Takei, A. C. Ford, Y. L. Chueh, and A. Javey, *Adv. Mater.* **21**, 3730 (2009).

<sup>4</sup>F. Xu, W. Lu, and Y. Zhu, *ACS Nano* **5**, 672 (2011).

<sup>5</sup>J.-Y. Lee, S. T. Connor, Y. Cui, and P. Peumans, *Nano Lett.* **8**, 689 (2008).

<sup>6</sup>J. J. Mock, S. J. Oldenburg, D. R. Smith, D. A. Schultz, and S. Schultz, *Nano Lett.* **2**, 465 (2002).

<sup>7</sup>A. Tao, F. Kim, C. Hess, J. Goldberger, R. He, Y. Sun, Y. Xia, and P. Yang, *Nano Lett.* **3**, 1229 (2003).

<sup>8</sup>W. Wang, Q. Yang, F. Fan, H. Xu, and Z. L. Wang, *Nano Lett.* **11**, 1603 (2011).

<sup>9</sup>H. S. Park and X. Qian, *J. Phys. Chem. C* **114**, 8741 (2010).

<sup>10</sup>B. Wu, A. Heidelberg, J. J. Boland, J. E. Sader, X. Sun, and Y. Li, *Nano Lett.* **6**, 468 (2006).

<sup>11</sup>G. Y. Jing, H. L. Duan, X. M. Sun, Z. S. Zhang, J. Xu, Y. D. Li, J. X. Wang, and D. P. Yu, *Phys. Rev. B* **73**, 235409 (2006).

<sup>12</sup>X. Li, H. Gao, C. J. Murphy, and K. K. Caswell, *Nano Lett.* **3**, 1495 (2003).

<sup>13</sup>M. Lucas, A. M. Leach, M. T. McDowell, S. E. Hunyadi, K. Gall, C. J. Murphy, and E. Riedo, *Phys. Rev. B* **77**, 245420 (2008).

<sup>14</sup>A. M. Leach, M. McDowell, and K. Gall, *Adv. Funct. Mater.* **17**, 43 (2007).

<sup>15</sup>C. L. Johnson, E. Snoeck, M. Ezcurdia, B. Rodriguez-Gonzalez, I. Pastoriza-Santos, L. M. Liz-Marzan, and M. J. Htych, *Nat. Mater.* **7**, 120 (2008).

<sup>16</sup>H. Chen, Y. Gao, H. Zhang, L. Liu, H. Yu, H. Tian, S. Xie, and J. Li, *J. Phys. Chem. B* **108**, 12038 (2004).

<sup>17</sup>Y. Zhu, F. Xu, Q. Qin, W. Y. Fung, and W. Lu, *Nano Lett.* **9**, 3934 (2009).

<sup>18</sup>F. Xu, Q. Qin, A. Mishra, Y. Gu, and Y. Zhu, *Nano Research* **3**, 271 (2010).

<sup>19</sup>Y. Zhu, Q. Qin, Y. Gu, and Z. Wang, *Nanoscale Res. Lett.* **5**, 291 (2010).

<sup>20</sup>Y. Zhu and H. D. Espinosa, *Proc. Natl. Acad. Sci. USA* **102**, 14503 (2005).

<sup>21</sup>S. Ogata, J. Li, N. Hirotsuki, Y. Shibusaki, and S. Yip, *Phys. Rev. B* **70**, 104104 (2004).

<sup>22</sup>M. D. Uchic, P. A. Shade, and D. M. Dimiduk, *Annu. Rev. Mater. Res.* **39**, 361 (2009).

<sup>23</sup>J. R. Greer and J. T. M. D. Hosson, *Prog. Mater. Sci.* **56**, 654 (2011).

<sup>24</sup>T. Zhu, J. Li, A. Samanta, A. Leach, and K. Gall, *Phys. Rev. Lett.* **100**, 025502 (2008).

<sup>25</sup>A. T. Jennings, J. Li, and J. R. Greer, *Acta Mater.* **59**, 5627 (2011).

<sup>26</sup>R. Agrawal, B. Peng, and H. D. Espinosa, *Nano Lett.* **9**, 4177 (2009).

<sup>27</sup>T. Zhu and J. Li, *Prog. Mater. Sci.* **55**, 710 (2010).

<sup>28</sup>A. Cao and Y. G. Wei, *Phys. Rev. B* **74**, 214108 (2006).

<sup>29</sup>S. S. Brenner, *J. Appl. Phys.* **27**, 1484 (1956).

<sup>30</sup>A. Rinaldi, P. Peralta, C. Friesen, and K. Sieradzki, *Acta Mater.* **56**, 511 (2008).

<sup>31</sup>G. Richter, K. Hillerich, D. S. Gianola, R. Monig, O. Kraft, and C. A. Volkert, *Nano Lett.* **9**, 3048 (2009).

<sup>32</sup>T. H. Courtney, *Mechanical Behavior of Materials* (McGraw Hill, Boston, 2000), p. 59.

<sup>33</sup>S. Cuenot, C. Fretigny, S. Demoustier-Champagne, and B. Nysten, *Phys. Rev. B* **69**, 165410 (2004).

<sup>34</sup>H. S. Park, W. Cai, H. D. Espinosa, and H. Huang, *MRS Bull.* **34**, 178 (2009).

<sup>35</sup>L. G. Zhou and H. Huang, *Appl. Phys. Lett.* **84**, 1940 (2004).

<sup>36</sup>H. Liang, M. Upmanyu, and H. Huang, *Phys. Rev. B* **71**, 241403 (2005).

- <sup>37</sup>G. Wang and X. Li, *J. Appl. Phys.* **104**, 113517 (2008).
- <sup>38</sup>H. S. Park and P. A. Klein, *J. Mech. Phys. Solids* **56**, 3144 (2008).
- <sup>39</sup>J. H. Yoo, S. I. Oh, and M. S. Jeong, *J. Appl. Phys.* **107**, 094316 (2010).
- <sup>40</sup>C. R. Weinberger and W. Cai, *J. Mater. Chem.* (in press), doi: [10.1039/c2jm13682a](https://doi.org/10.1039/c2jm13682a).
- <sup>41</sup>C. Q. Chen, Y. Shi, Y. S. Zhang, J. Zhu, and Y. J. Yan, *Phys. Rev. Lett.* **96**, 075505 (2006).
- <sup>42</sup>R. Agrawal, B. Peng, E. E. Gdoutos, and H. D. Espinosa, *Nano Lett.* **8**, 3668 (2008).
- <sup>43</sup>M. R. He, P. Xiao, J. Zhao, S. Dai, F. Ke, and J. Zhu, *J. Appl. Phys.* **109**, 123504 (2011).
- <sup>44</sup>C. A. Volkert and E. T. Lilleodden, *Phil. Mag.* **86**, 5567 (2006).
- <sup>45</sup>C. P. Frick, B. G. Clark, S. Orso, A. S. Schneider, and E. Arzt, *Mater. Sci. Eng. A* **489**, 319 (2008).
- <sup>46</sup>D. Kiener and A. M. Minor, *Acta Mater.* **59**, 1328 (2011).
- <sup>47</sup>H. S. Park, K. Gall, and J. A. Zimmerman, *J. Mech. Phys. Solids* **54**, 1862 (2006).
- <sup>48</sup>H. Zheng, A. Cao, C. R. Weinberger, J. Y. Huang, K. Du, J. Wang, Y. Ma, Y. Xia, and S. X. Mao, *Nat. Commun.* **1**, 144 (2010).
- <sup>49</sup>A. T. Jennings and J. R. Greer, *Phil. Mag.* **91**, 1108 (2010).
- <sup>50</sup>Y. T. Zhu, X. L. Wu, X. Z. Liao, J. Narayan, L. J. Kecskes, and S. N. Mathaudhu, *Acta Mater.* **59**, 812 (2011).
- <sup>51</sup>E. Ma, Y. M. Wang, Q. H. Lu, M. L. Sui, L. Lu, and K. Lu, *Appl. Phys. Lett.* **85**, 4932 (2004).
- <sup>52</sup>K. Lu, L. Lu, and S. Suresh, *Science* **324**, 349 (2009).
- <sup>53</sup>C. Deng and F. Sansoz, *Nano Lett.* **9**, 1517 (2009).